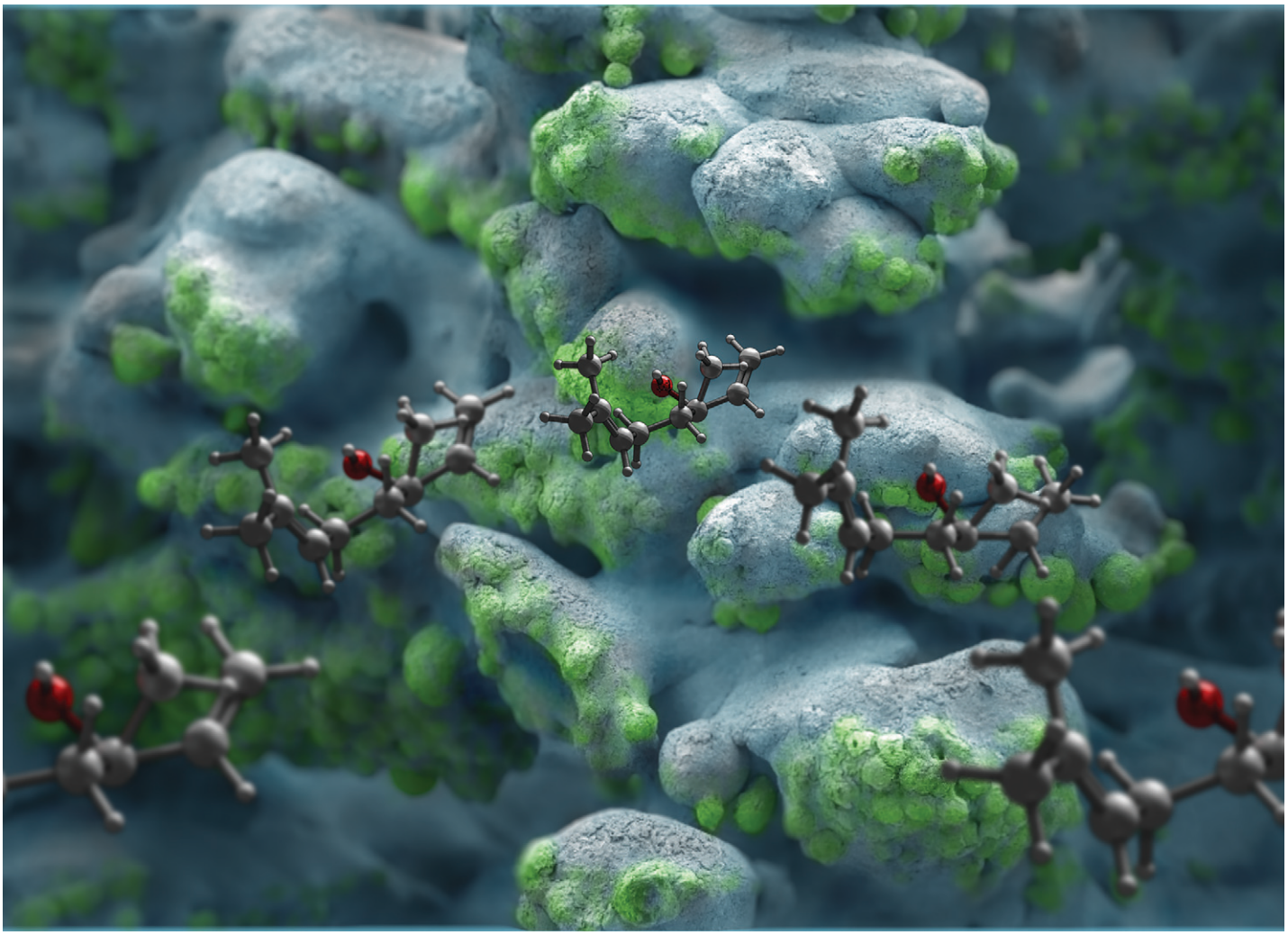

Showcasing research by the FloWorks Group led by Christian Hornung at the Commonwealth Scientific & Industrial Research Organisation (CSIRO) in Melbourne, Australia.

3D printed nickel catalytic static mixers made by corrosive chemical treatment for use in continuous flow hydrogenation

A new approach combining additive (3D metal printing) and subtractive (chemical etching) methods to generate a novel class of structured nickel catalysts used for the selective hydrogenation of flavourings & fragrances.

The authors thank Fletcher Wollard for the creation of this cover image.

As featured in:

See Christian H. Hornung *et al.*, *React. Chem. Eng.*, 2022, **7**, 284.

ROYAL SOCIETY OF CHEMISTRY

rsc.li/reaction-engineering

Registered charity number: 207890

Reaction Chemistry & Engineering

ROYAL SOCIETY OF CHEMISTRY

PAPER

View Article Online
View Journal | View Issue

Check for updates

Cite this: *React. Chem. Eng.*, 2022, **7**, 284

3D printed nickel catalytic static mixers made by corrosive chemical treatment for use in continuous flow hydrogenation†

Milan Kundra, Yutong Zhu, Xuan Nguyen, Darren Fraser, Christian H. Hornung * and John Tsanaktsidis

Received 16th October 2021,
Accepted 15th November 2021

DOI: 10.1039/d1re00456e

rsc.li/reaction-engineering

Catalytic static mixers, 3D printed from nickel alloys, were treated with etching or leaching solutions to activate their surfaces for use in hydrogenation of alkenes, aldehydes and nitro-groups. Their performance was benchmarked against industrial standard alumina catalysts, using a tubular continuous flow reactor. These novel structured catalysts were additively manufactured from printer-grade Monel and Inconel powders. Especially the Monel-type catalysts, consisting predominantly of nickel and copper by weight, presented a surface layer significantly enriched in nickel after the leaching protocol, which resulted in a high catalytic activity and a surprising selectivity towards unsubstituted double bonds.

Introduction

Over the past decade, 3D printing has been used by numerous research groups to create new structured catalysts for use in heterogeneous catalysis applications.[1–26] While many of these additively manufactured catalysts were employed in batch in the laboratory, the real potential for 3D-printed structured catalysts lies in their use in industrial continuous flow processes, improving the intensity and performance of established reactor systems such as fixed beds. Hurt *et al.*,[4] Rossi *et al.*,[5] and Parra-Cabrera *et al.*[6] have presented reviews of 3D-printed catalysts for reactions used in the manufacture of pharmaceuticals, fine and bulk chemicals, food products and others, and we have further referenced recent additions to the field in our latest publications.[12,27]

Our work on 3D printed structured catalysts has focused on the use in catalytic hydrogenations. For this we have investigated the performance of catalytic static mixers (abbr. CSMs), which are 3D-printed metal mixer scaffolds, coated with an active catalyst layer, that can be inserted into a continuous flow reactor. Over the past years we have used CSMs for a range of different hydrogenation applications, such as the reduction of nitro groups[28–30] which are commonly used in API manufacture, the hydrogenation of alkenes and carbonyls for the production of flavourings and fragrances,[27] the reduction of fatty acids,[31] the semi-hydrogenation of alkynes[12] and in reductive aminations.[32] In all these cases the CSMs were manufactured in two steps: 1) 3D printing of mixer scaffold, 2) deposition of a catalytically active layer by means of electroplating, metal cold-spraying or wash-coating.

The method presented herein uses the same additive manufacturing process to form the mixer, followed by a subtractive manufacturing method, consisting of removal of sacrificial material from the surface layer by chemical etching or leaching, thereby activating the surface for chemical catalysis. This is an intrinsically new method to build these 3D printed structured catalysts and requires the use of printable metal powders that contain the catalytically active metals in an alloyed form. In our work we have used printer-grade Inconel and Monel powders, both of which contain high amounts of nickel that can be made catalytically active following wet chemical etching or leaching. The combination of the additive and subtractive manufacturing steps is instrumental for the performance of the CSM in heterogeneous catalytic applications, such as hydrogenations. Herein, we evaluate these Ni-CSMs for a range of test hydrogenation reactions, including the reduction of alkenes, aldehydes, and nitro groups. Different to most standard nickel catalysts, such as powder-form or pelletised Ni/Al_2O_3 or RANEY® nickel, our catalysts are made from industry standard nickel base alloys such as Monel and Inconel, which are widely used as materials of construction in chemical apparatus. The preparation of these Ni-CSMs uses cost effective and common inorganic chemicals which is in stark contrast to the manufacture of most other nickel catalysts which often are made from expensive precursor materials and require the use of complex porous support materials, binders, ligands or other additives.

CSIRO Manufacturing, Bag 10, Clayton South, Victoria 3169, Australia.
E-mail: christian.hornung@csiro.au

† Electronic supplementary information (ESI) available. See DOI: 10.1039/d1re00456e

Experimental

In the following, we describe a new method to prepare 3D-printed structured catalysts which can be used as inserts for tubular flow reactors. A prerequisite for this methodology is the ability to print metal alloys that can be made catalytically active by using a subsequent wet chemical process, meaning that the printing powder has to contain a catalytically active metal as a major or minor component. To date, several Ni-base alloy powders have been manufactured commercially for 3D printing, including Monel (alloy 400),[33] Hastelloy (alloy C276, alloy X),[34] Inconel (alloy 625, alloy 718, alloy 738)[35] and more. After being printed into the desired shape, the metallic structure is then subjected to a corrosive environment, in order to create a nickel-rich surface layer with increased porosity and enhanced surface area, ultimately resulting in improved catalytic activity. The preparation sequence is illustrated in Fig. 1.

The above diagram makes a distinction between a 'leaching process' and an 'etching process' for the subtractive manufacturing step. In general terms, we define leaching as the selective removal of a sacrificial metal phase, achieved here *via* dissolution from the printed alloy matrix, while leaving the 'desired' catalytically active metal species (in this case Ni) intact and in place. In this study, we selectively leached Cu from Monel, an alloy consisting principally of Ni and Cu. The resulting leached surface layer is porous, enriched in nickel and depleted in copper.

In comparison, etching removes and/or oxidises several metal species from the printed alloy matrix by dissolving them from the surface in relatively equal amounts. This treatment creates a top layer with a greatly increased porosity and surface area, while being non-selective with respect to the individual metal species of the alloy. An example is the non-selective removal of Ni and Cr from Inconel, the two main components of this alloy by weight. The resulting etched layer is porous, but not significantly enriched in either Ni or Cr.

In both the leaching and the etching procedure, the treatment is topical and will have a limited penetration depth into the printed part but will at the same time greatly increase the surface area and porosity within that newly formed layer, leading to much enhanced catalytic activity.

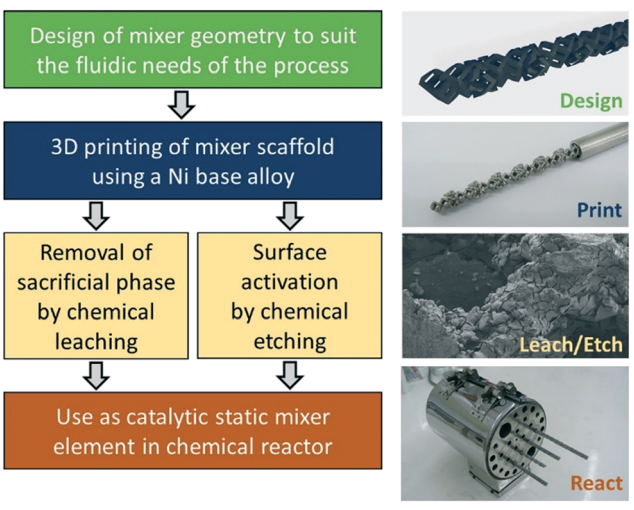

Fig. 1 Workflow scheme for the preparation of catalytic static mixers made by a chemical etching or leaching treatment.

Materials

Printer grade Inconel powder (alloy 738) was sourced from Praxair. This powder had a metal composition of ~61% Ni, 16% Cr, 8.5% Co, 3.4% Al, 3.4% Ti, 2.6% W, 1.8% Ta, 1.8% Mo, and smaller amounts of Fe, C, B, Zr, Mn, Si and S. Printer grade Monel powder (alloy 400) was sourced from Micron Metals. This powder had a metal composition of ~61% Ni, 35% Cu, 2.2% Fe, 1.3% Mn and 0.5% Si.

The following solvents and chemicals were used in this study: ethanol (absolute) was obtained from Merck; vinyl acetate (VAc), cinnamaldehyde (CAL), 2,5-dichloro nitro benzene (DCNB) and β-myrcene were purchased from Sigma Aldrich; coumarin, (−)-isopulegol and linalool (LOL) were purchased from Perfumers world ltd. all solvents and reagents were used as received without further purification.

Preparation of nickel-type catalytic static mixers from Inconel

Nickel-type catalytic static mixers additively manufactured from Inconel (termed Ni-Inc) were printed on the Arcam A1 electron beam melting 3D printer using Praxair powder. The machine process parameters were set by trial for this powder. Arcam electron beam melting (EBM) uses an electron beam to melt and fuse metal powders, layer-by-layer, into three-dimensional parts. The process takes place under vacuum in a powder bed where a rake feeds a layer of powder over a starting plate on a vertically movable table. A typical starting bed temperature for Inconel is 1050 °C. This is to lightly sinter and stabilise the powder as it builds. Supports underneath the CSM scaffolds were built; these were 0.5 mm diameter and 3 mm long support pillars that aid in the melting process to avoid swelling of the part above the plane of the powder layer. A 'net' theme is used for the melting of the mixers due to their fine cross-sections. At the end of the build the unfused lightly sintered powder is removed from around the mixer by grit-blasting with the same powder material.

The printed static mixers were then subjected to a chemical etching solution, namely Marble's reagent, a solution of 1 M $CuSO_4$ in 4.4 M aqueous HCl.[36] This reagent was selected after first trialling various other etchants. First, small Inconel samples were tested over several etching periods, with the etching times set to 5 min, 20 min, 2 h, 24 h or 48 h (at room temperature), yielding different surface topographies. Each treated sample was washed with copious amounts of water and then ethanol before blow-drying with nitrogen. The mass loss for these samples was relatively low

and after the first 2 min of exposure to the solution, the Inconel samples had lost only ~0.05% of their weight.

After these initial etching tests with varying treatment times were completed and results were evaluated, we decided to prepare a full set of four Inconel mixers using 250 mL Marble's reagent and an etching time of 24 h at room temperature. This treatment resulted in surface etching and partial oxidation of Ni, Cr and other metal species within the alloy. Upon an additional reduction/activation procedure, to reduce Ni-oxides to Ni[0], this CSM could be used as a Ni[0] type catalyst for hydrogenation reactions.

Preparation of nickel-type catalytic static mixers from Monel

Nickel-type catalytic static mixers prepared from Monel (termed Ni-Mon) were printed on the Arcam A1 electron beam melting 3D printer using Micron Metals powder. The machine process parameters were set by trial for this powder. A typical starting bed temperature for Monel is 600 °C to lightly sinter the powder as it builds. Supports underneath the CSM scaffolds were built; these were 0.5 mm diameter and 3 mm long support pillars that aid in the melting process to avoid swelling of the part above the plane of the powder layer. A 'net' theme is used for the melting of the mixers due to their fine cross-sections. At the end of the build the lightly sintered unfused powder is removed from the mixer by grit-blasting with the same powder material.

The static mixers were then subjected to a chemical leaching protocol, not only to increase the porosity of the surface but also to selectively remove the copper. Four Monel mixers were added to a 450 mL of an aqueous solution of 2M ammonium sulfate and 5M ammonia and left for 10 days, applying sonication for a minimum of 1 h per day. *Ca.* 30 mL of aqueous ammonia was added once every three days to replace ammonia lost as gas. The mixture was observed to turn a pale green. The mixers were then washed thoroughly in water and added to a separate 450 mL aqueous solution of 2M ammonium persulfate and 5M ammonia. They were left in this solution for another 12 days, applying the same sonication and ammonia top-up protocol as above. The persulfate mixture was observed to turn a sapphire blue, the colour of $[Cu(NH_3)(OH_2)_2]^{2+}$, (see Fig. 2). The leaching solutions used were selected from the literature.[37] The CSMs were then washed with copious amounts of water and then ethanol, before being air-dried over four days.

In contrast to the treatment of the Inconel static mixers, this leaching protocol predominantly removed copper from the printed parts, enriching the remaining layer in nickel. The resulting Ni/Cu ratio at the surface of the CSM was between 4 and 8 after treatment, compared to 1.77 in the untreated sample. After activation, the CSM could be used as a Ni[0] type catalyst for hydrogenation reactions. Fig. 3 shows a set of Inconel and Monel CSMs before (Ni-Inc-UT & Ni-Mon-UT) and after (Ni-Inc & Ni-Mon) the etching/leaching treatment.

Catalyst activation & catalyst loading

Each set of CSMs was activated using hydrogen after the chemical treatment. The activation process reduces the catalytically deactivating metal oxides formed by aerobic passivation. To identify the necessary conditions, temperature-programmed reduction (TPR) was performed on small cut-offs of the printed Ni-Inc and Ni-Mon CSMs. This involves passing a constant stream of 95% N_2/5% H_2 over the catalyst in a furnace, with a steady temperature ramp from 20 °C to the desired maximum temperature (up to 800 °C). The activation protocol chosen for both Ni-Inc and Ni-Mon was 24 bar, 200 °C at a liquid flow of ethanol of 0.05 mL min^{-1} and a hydrogen flow of 100 mL_N min^{-1}. This activation procedure was conducted for 24 h for each CSM set.

The performance of the Ni-Inc and Ni-Mon CSMs was benchmarked against CSMs made by additive coating processes, namely a set of cold-sprayed Ni CSMs (abbr. Ni-CS) and CSMs wash-coated with Ni/Al_2O_3 (abbr. Ni-AO), Pd/Al_2O_3 (abbr. Pd-AO) or Pt/Al_2O_3 (abbr. Pt-AO), described in earlier work. For these CSMs, the static mixer was printed from 316 L stainless steel powder and then the catalytic layer was deposited by the spray or dip-coat process. Our team has developed several of these coating processes over the past years and evaluated their performance in a series of hydrogenation applications; detailed preparation protocols

Fig. 2 Leaching solution for the treatment of the Monel CSMs, after 12 h of treatment, the sapphire blue colour stems from the $[Cu(NH_3)(OH_2)_2]^{2+}$ formed.

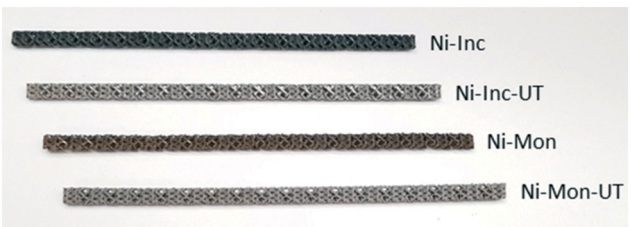

Fig. 3 Photo of Inconel and Monel CSMs before and after treatment: Ni-Inc, Ni-Inc-UT, Ni-Mon and Ni-Mon-UT.

and performance evaluation data can be found in earlier work.[28,29]

Each CSM had a diameter of 6 mm and length of 150 mm. The six catalyst sets (containing 4 CSMs each) that were compared in this study, had the following average nickel/palladium/platinum loadings:

- Ni-Inc: 68.73 mmol Ni per CSM
- Ni-Mon: 81.59 mmol Ni per CSM
- Ni-CS: 8.50 mmol Ni per CSM
- Ni-AO: 0.40 mmol Ni per CSM
- Pd-AO: 0.15 mmol Pd per CSM
- Pt-AO: 0.10 mmol Pt per CSM

It should be stated here that for Ni-Inc, Ni-Mon and Ni-CS large proportions of the Ni species are locked away inside the 3D printed scaffold or inside the cold-sprayed Ni layer and are believed to be not accessible for the fluids passing through the hydrogenation reactor. Only Ni at or close to the surface is believed to be available for catalysis. The ratio of available to non-available catalytic metal for the aluminium oxide-coated CSMs (suffixed-AO) is substantially higher than for cold-sprayed and directly printed CSMs, as the metals are present in the form of alumina-supported nanoparticles, which are well-known to bear larger surface areas than traditional metal surfaces.[38] It should be noted that the much higher nickel content used in the Ni-Mon and Ni-Inc CSMs is not necessary a disadvantage of this approach and has the potential to be more cost-effective than using expensive preformed nickel catalyst powders such as Ni/Al_2O_3. Both Inconel 738 and Monel 400 are commonly used engineering alloys, widely employed in the construction of reactor apparatus and other process equipment, that require enhanced stability against chemical attack. Our manufacturing method also reduces manufacturing steps as both the mixer scaffold and the catalytically active top layer are made from the same material. This has the potential to greatly reduce manufacturing costs, as expensive coating processes are not required. Using Monel or Inconel as the load bearing scaffold material of the CSM also has the additional advantage that the whole part is chemically much more resistant than our standard stainless-steel based CSMs. Both Ni-base alloys are rated for use in corrosive environments including oxidising acids, such as nitric acid, reducing acids, such as sulphuric and hydrochloric acid, and alkali media, such as aqueous sodium hydroxide (see: Product Handbook of High-Performance Nickel Alloys, https://www.specialmetals.com/products/). This greatly increases the operational window for these CSMs compared to their stainless-steel counterparts, and enables their use for hydrogenations at extreme pH, both high and low. Naturally, also all other wetted parts in the reactor system need to match the chemical compatibility and requires the use of appropriate materials of construction, including the reactor housing, tubing valves and other instrumentation. As we have utilised the common engineering alloys Monel 400 and Inconel 738, these solutions and components are readily available and considered industry standard.

Continuous flow hydrogenation experiments

A series of continuous flow hydrogenation experiments with gaseous hydrogen were conducted using a tubular CSM reactor, capable of operating up to 12 CSMs in series (each with a diameter of 6 mm and a length of 150 mm). The reactor and its general operation has been described in our previous work.[29]

Control experiments were undertaken with untreated Inconel and Monel CSMs to investigate the effect of the etching/leaching procedure on the activity of the mixer. These untreated control CSM sets were labelled Ni-Inc-UT and Ni-Mon-UT and were subjected to the same activation protocol prior to reaction.

Several different target molecules were hydrogenated using the CSM reactor to evaluate performance; these substrates are shown in Fig. 4, in which the reactive moieties for each substrate are highlighted in red.

For a typical hydrogenation of vinyl acetate (VAc) using a set of the above mentioned CSMs, the following experimental protocol was employed:

Before first use of the CSMs, they were activated inside the reactor by flowing hydrogen over them at 24 bar, 120 °C and a gas flow rate of 200 mL_N min^{-1}. The activation was conducted for a minimum of 6 h. After activation the reactor was flushed with solvent ethanol (EtOH), using the liquid reagent pump. A substrate solution containing 2 M of VAc in EtOH was prepared. During start-up of the reactor, hydrogen gas was introduced, together with the washing solvent (EtOH) to prime the reactor, and the parameters for the reaction were adjusted to the following: reactor pressure, p_R = 20 bar, liquid flow rate, L = 1 ml min^{-1}, gas flow rate inside the reactor at reaction pressure, G_R = 4 mL min^{-1}, normal gas flow rate (measured by the hydrogen mass flow controller), G_N = 54.4 mL_N min^{-1}, reactor temperature, T_R = 120 °C.

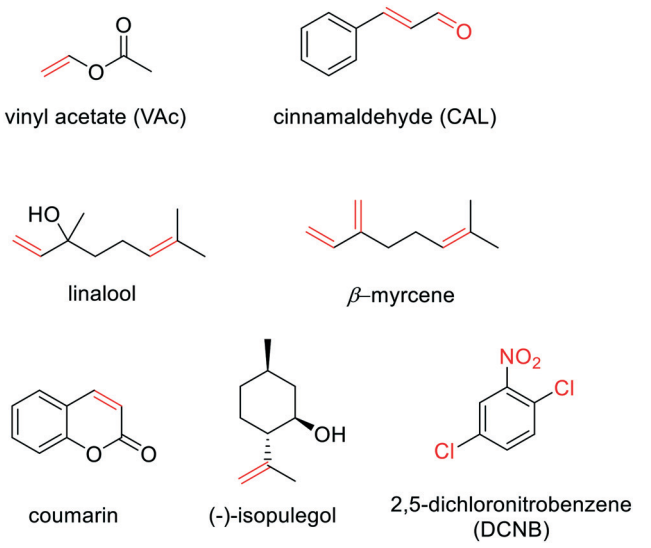

Fig. 4 Substrates for the hydrogenation experiments using the CSM reactor.

These settings equate to a volumetric gas to liquid ratio, G/L, of 4, and a molar hydrogen to substrate ratio, H/S, of 1.11.‡ Once pressure and temperature had stabilised, the liquid feed was changed from solvent to stock solution, thus starting the reaction. After one residence time inside the reactor, the clear product, ethyl acetate in solvent, was collected at the outlet of the reactor and was then analysed by ^{1}H-NMR. To compare the time that the liquid phase travels through the reactor, we defined a liquid space time, ST_L, as follows:

$$ST_L = \frac{V_{\text{test section}}}{L} = \frac{\pi d^2 l}{4L} \quad (1)$$

Here L is the liquid flow rate, d the tube diameter and l the length of the CSM test section. For a set of 4 CSMs, the ST_L ranged from 17.0 min at 1 mL min^{-1} to 8.5 min at 2 mL min^{-1} and 3.4 min at 5 mL min^{-1}.

Some of the substrates contained only one reactive moiety, hence only one major product was observed. In examples where multiple (up to three) reactive moieties were present in the molecule, several product species were observed, containing partially hydrogenated intermediates as well as fully saturated products. Where the latter was the case, we either present a full product composition or a selectivity value towards the major product.

Characterisation methods

3D printed catalyst samples were imaged and characterised using scanning electron microscopy with energy-dispersive X-ray spectroscopy (SEM-EDX). First they were mounted on aluminium stubs with double-sided conductive carbon tape. The samples were imaged uncoated using a Hitachi TM3030Plus tabletop SEM. The images were obtained using the secondary electron (SE) mode and back-scattered mode (BSE). SE images highlight topographical features whereas BSE imaging enhances elemental contrast and oxidation state differences so that low atomic elements or oxidated elements appear darker and higher atomic number elements or in the elemental state appear brighter. Energy dispersive X-ray spectroscopy was used to identify elements present within the samples. The EDX system used was AZTEC, manufactured by Oxford Instruments Pty Ltd. An accelerating voltage of 15 kV was used for imaging and EDX analysis. The results are to be taken as semi-quantitative and only trends compared. The magnifications used are indicative of the scale bars shown in the images.

X-ray photoelectron spectroscopy (XPS) analysis was performed using an AXIS Nova spectrometer (Kratos Analytical Inc., Manchester, UK) with a monochromated Al Kα source at a power of 180 W (15 kV × 12 mA) and a hemispherical analyser operating in the fixed analyser transmission mode. The total pressure in the main vacuum chamber during analysis was typically between 10–9 and 10–8 mbar. Survey spectra were acquired at a pass energy of 160 eV and step size 0.5 eV. Data processing was performed using CasaXPS processing software version 2.3.15 (Casa Software Ltd., Teignmouth, UK). All elements present, were identified from survey spectra. The atomic concentrations of the detected elements were calculated using integral peak intensities and the sensitivity factors supplied by the manufacturer.

Nuclear magnetic resonance (NMR) experiments were performed on Bruker Avance 400 and/or 500 MHz NMR spectrometers. NMR experiments were performed with the sample held at 25 ± 0.1 °C. Chemical shifts for all experiments are referenced using the Unified Scale relative to 0.3% tetramethylsilane in deuterochloroform (ref. 1 and 2). Samples for NMR spectroscopy were prepared by dissolving the analyte in deuterated solvent, as specified, and placing the solution into a 5 mm NMR tube. The data were processed using Bruker TopSpin v3.6.2 software.

Temperature programmed reduction (TPR) analysis was performed using a PSs Micromeritics Chemisorb 2750 TPx system at a ramping rate of 10 °C min^{-1} to 800 °C. The amount of the analysed catalyst sample was 50 mg and the consumption of hydrogen by adsorption/reaction was monitored and calculated using Chemisoft TPx software.

Results and discussion

Characterisation of the Ni surfaces

First, we investigated the etching approach using 3D printed Inconel samples, using SEM-EDX to characterise the treated samples. For this, small 3D printed Inconel samples were subjected to a range of corrosive solutions with the aim to pit the surface layer, which would increase the exposed surface area, and in turn the catalytic activity. After investigating a series of acidic solutions and settling on Marble's reagent, we ran time trials, wherein samples were exposed to the etching solution for time periods between 5 min and 48 h, and then characterised by SEM-EDX. The SEM images from these experiments are shown in Fig. 5 and the elemental composition in Table 1.

The images in Fig. 5 show the progression of the acid etching over time, with a general pitting of the surface layer observable after only a few minutes, and a more severe cracking and peeling effect of said top layer occurring after several hours. The elemental compositions in Table 1 reveal no significant selective removal process; instead, they point to the occurrence of oxidation. The ratio of main metal constituents of the alloy, Ni, Cr, Co, Ti and Al, remain essentially the same, however, the amount of oxygen increases significantly from only trace amounts to >10%. This is a clear indication of the formation of oxides, which coincides with the change in visual appearance of the samples, from shiny metallic to black (see also Fig. 3).

‡ Note that the calculation of G/L is based on the gas flow rate at reactor pressure, G_R, not the normal gas flow rate, G_N.

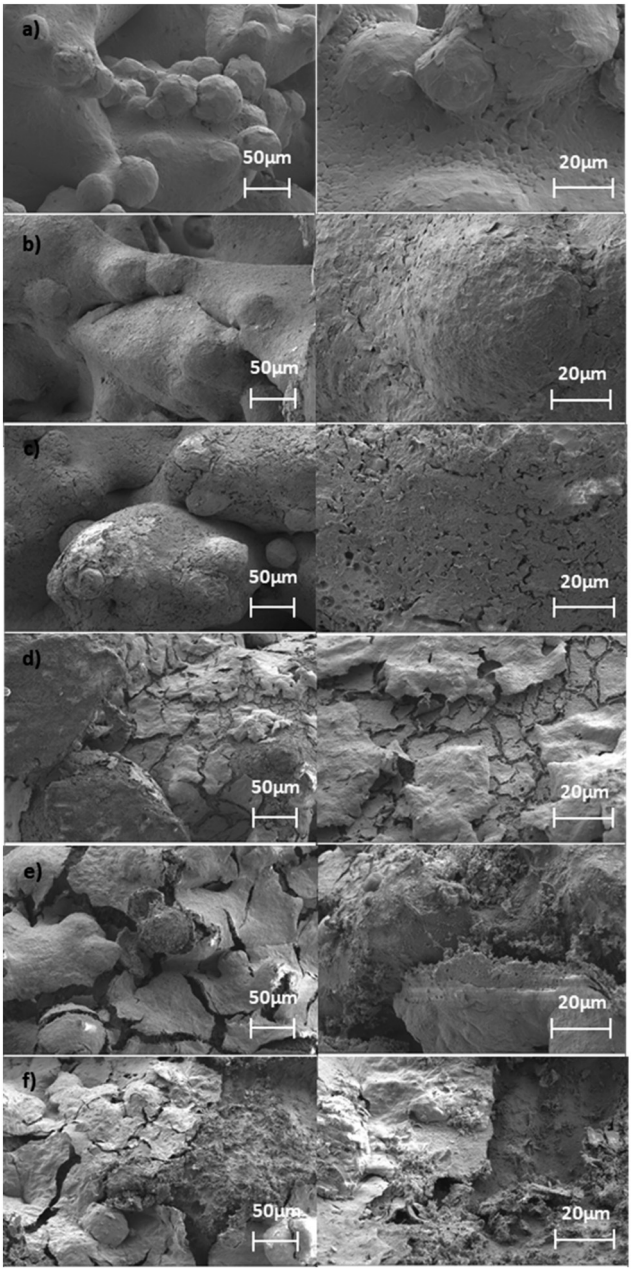

Fig. 5 SEM images of Inconel samples at various etching times. Each row contains images of the same sample at two different magnifications (left: 250× and right: 1000×) a) untreated Inconel; b) etched Inconel after 5 min; c) etched Inconel after 20 min; d) etched Inconel after 2 h; e) etched Inconel after 24 h; f) etched Inconel after 48 h.

Next, we investigated the leaching approach using 3D printed Monel samples. Firstly, we tested several leaching solutions for their effectiveness to selectively remove Cu from the 3D printed Monel test samples. SEM-EDX was used to characterise samples before and after leaching in order to test for nickel enrichment and copper depletion. For this first pass, we considered a range of different leachants, including the following: sulphuric acid, nitric acid, hydrochloric acid, oxalic acid, acidic acid, sodium sulfate, sodium nitrate,

Table 1 Elemental composition of the surface layer of Inconel samples after various etching times, as determined by EDX

	wt%					
Element	0 min	5 min	20 min	2 h	24 h	48 h
Ni	56	44	37	39	33	36
Cr	14	15	12	13	10	13
Co	8	6	5	5	4	5
Ti	4	3	4	3	5	4
Al	3	3	3	2	1	2
O	2	7	9	8	14	12

sodium chloride, ammonium sulfate, ammonium nitrate, ammonium chloride, ammonium thiosulfate, ammonium carbonate and ammonium persulfate. These leachants were investigated as 1 M strong aqueous solutions, with or without the addition of 5 M aqueous ammonia. For the majority of the solutions, no selective removal of Cu was observed and the Ni/Cu ratio remained similar to an untreated sample. Whilst some of the strong acids such as hydrochloric acid removed both Cu and Ni in noticeable amounts, some of the weaker acids such as acetic acid hardly removed any metal at all. The two candidates that looked the most promising from these early tests were ammonium persulfate with 5 M ammonia and ammonium sulfate with 5 M ammonia. We then conducted further in-depth leaching experiments with these two leachant solutions. These tests consisted of timed trials, wherein the mass loss was studied gravimetrically over a period of 8 days (see Table 2), as well as further examination of the surface compositions of these samples after leaching using XPS (see Table 3).

From Table 2, it can be observed that there is a strong time dependency on the leaching process, with between 1 and 4% of the total mass of the sample being eroded away after 8 days in the respective solutions. Ammonium persulfate proved more aggressive than ammonium sulfate at the same concentration, and increasing concentration to a 1 M persulfate solution resulted in more than twice the mass loss than the weaker 0.2 M persulfate solution after 8 days. Fig. 6 shows SEM images of the samples from Table 2, depicting the changes in surface morphology. Compared to the pitting and peeling effects of the acid treatment conducted for the Inconel samples, the impact of the ammonia treatments was

Table 2 Mass loss of Monel samples after various leaching treatments and times, determined gravimetrically

Leachant	Time [d]	Δm [mg]	Δm [%]
0.2 M ammonium persulfate in 5 M aqueous NH_3	1	1.6	0.29
	3	5.9	0.92
	8	10.4	1.56
1 M ammonium persulfate in 5 M aqueous NH_3	1	7.4	1.25
	3	6.7	1.04
	8	28.2	4.19
1 M ammonium sulfate in 5 M aqueous NH_3	1	2.1	0.35
	3	5.8	0.88
	8	6.7	0.98

Table 3 Nickel to coper ratio, Ni/Cu, of the surface layer of Monel samples after various leaching treatments and times, determined by XPS; detailed composition data from these XPS measurements can be found in the ESI†

Leachant	NH_3	Time [d]	Ni/Cu
0.2 M ammonium persulfate	5 M	7	6.51
0.5 M ammonium persulfate	5 M	3	5.78
0.5 M ammonium persulfate	7 M	7	5.06
1 M ammonium persulfate	7 M	7	7.83
1 M ammonium sulfate	7 M	7	4.22
Untreated Monel	—	—	1.76
Monel (theoretical – based on information from supplier)			*1.74*

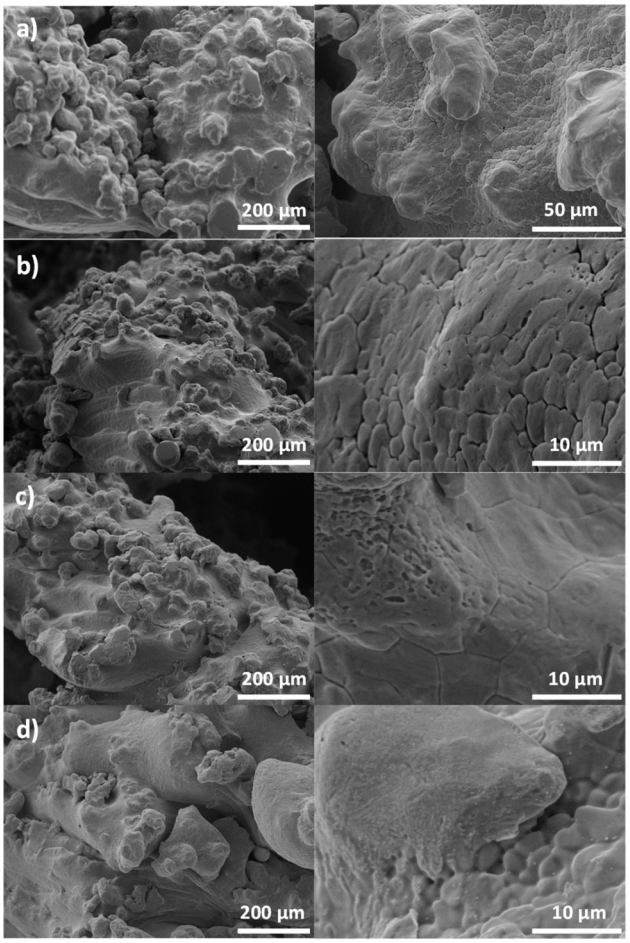

Fig. 6 SEM images of Monel samples after 8 days of etching in different ammonia solutions (see also Table 2). Each row contains images of the same sample at two different magnifications (left: 200× and right: 5000×) a) untreated Monel; b) 0.2 M ammonium persulfate; c) 1 M ammonium persulfate; d) 1 M ammonium sulfate.

much milder, but nevertheless shows a general roughening of the surface after extended exposure.

Table 3 compares different ammonia treatments for their effectiveness towards enriching the surface layer in nickel and depleting it in copper. As can be seen, the nickel to copper ratio at the surface, Ni/Cu, changed from 1.76 in untreated Monel to 7.83 after 7 days in 1 M ammonium persulfate solution and to 4.22 after 7 days in 1 M ammonium sulfate solution. This confirms that these treatments can result in selective removal of Cu from the surface layer, forming a porous matrix enriched in nickel and with an increased surface area. Ultimately, we decided to apply a combined 2-step treatment to our full set of four Monel CSMs. In the first step a solution of 2 M ammonium sulfate and 5 M ammonia was used and in the second 2 M ammonium persulfate and 5 M ammonia. Using the oxidising agent ammonium persulfate in this second step, generated mild oxidising conditions, though nowhere near as harsh as during the corrosive Marble's reagent treatment applied to the Inconel mixers. To quantify the catalytic activity of leached Monel, we performed a series of hydrogenation reactions.

Catalyst performance

We have investigated the performance of the chemically etched CSMs against a series of other Ni, Pd and Pt containing CSMs prepared using cold-spraying or wash-coating.[27,28] Table 4 shows a list of comparative reactions for the reduction of alkenes, carbonyls and nitro-groups on different Ni CSMS, including Ni-Inc, Ni-Mon and their untreated counterparts Ni-Inc-UT and Ni-Mon-UT, as well as Ni-CS and Ni-AO. Each catalyst set consisted of four standard CSMs with a length of 150 mm.

The data from Table 4 reveals that even untreated Inconel and Monel CSMs showed some activity for hydrogenation of these test molecules, albeit at a very low level. At the above conditions the nitro reduction of DCNB using untreated Monel CSMs yielded 23% conversion. However, the control experiments have shown that the chemical treatment protocols have resulted in a significant improvement of the activity of both catalysts; for both Ni-Inc and Ni-Mon, conversions have improved by a factor of ~6. For the hydrogenation of VAc, Ni-Mon showed a significantly higher activity than Ni-Inc; hence we mainly focused on investigating the Ni-Mon CSMs for the following hydrogenation reactions.

In the case of the hydrogenation of coumarin, the Ni-Mon catalysts performed well compared to its nickel counterparts Ni-CS and Ni-AO. While at low substrate flow rates of 1 mL min^{-1} it was outperformed by Ni-CS and Ni-AO, at higher substrate flow rates of 5 mL min^{-1} it produced comparable results. For the hydrogenation of linalool to 1,2-dihydrolinalool, the performance of Ni-Mon was also comparable to Ni-AO. For the substrates cinnamaldehyde and isopulegol its activity was significantly lower than the other two nickel CSMs.

The VAc reduction was studied in further detail, whereby the liquid flow rate was changed from 1 to 4 mL min^{-1}, in turn altering the hydrogen to substrate ratio, H/S, between 0.25 and 1.05. The results in Fig. 7 show this data plotted either over the liquid flow rate or H/S; the H/S graph also

Table 4 Conversion, X, and selectivity, S, for the continuous flow hydrogenation of selected model substrates using various Ni CSMs (each catalyst set contained four CSMs)

Product	Catalyst	Solvent	L [mL min^{-1}]	H/S [mol mol^{-1}]	X [%]	S [%]
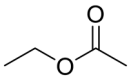	Ni-Inc	EtOH[a]	1	1	54	~100
	Ni-Inc-UT	*EtOH*[a]	*1*	*1*	*9*	*~100*
	Ni-Mon	EtOH[a]	1	1	95	~100
	Ni-Mon-UT	*EtOH*[a]	*1*	*1*	*31*	*~100*
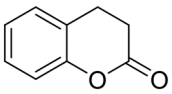	Ni-Mon	EtOAc	1	5	57	~100
	Ni-Mon	EtOAc	5	5	34	~100
	Ni-Mon-UT	*EtOAc*	*1*	*5*	*4*	*~100*
	Ni-Mon-UT	*EtOAc*	*5*	*5*	*0*	*N/A*
	Ni-CS	EtOAc	1	5	98	~100
	Ni-CS	EtOAc	5	5	13	~100
	Ni-AO	EtOAc	1	5	80	~100
	Ni-AO	EtOAc	5	5	42	~100
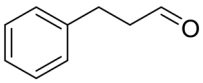	Ni-Mon	EtOAc	2	5	37	50
	Ni-Mon-UT	*EtOAc*	*2*	*5*	*13*	*N/A*
	Ni-CS	EtOAc	2	5	79	75
	Ni-AO	EtOAc	2	5	57	88
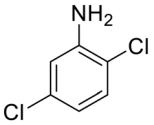	Ni-Mon	EtOH[b]	2	50	70	~100
	Ni-Mon-UT	*EtOH*[b]	*2*	*50*	*23*	*~100*
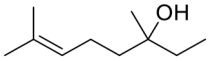	Ni-Mon	EtOAc	2	5	95	~100
	Ni-AO	EtOAc	2	5	~100	62
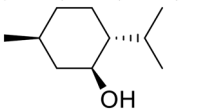	Ni-Mon	EtOAc	2	5	12	~100
	Ni-CS	EtOAc	2	5	83	~100
	Ni-AO	EtOAc	2	5	82	~100

For all reactions the reactor pressure was set to 24 bar, the temperature to 120 °C and the substrate concentration to 0.5 mol L^{-1} unless stated otherwise; when L was increased, the hydrogen flow rate was also increased accordingly to yield the same H/S. [a] Substrate concentration: 2 mol L^{-1} & reactor pressure: 20 bar. [b] Substrate concentration: 0.05 mol L^{-1}.

contains a dashed line marking the theoretical maximum that can be achieved at the given H/S ratio. These results demonstrate that for a simple terminal alkene reduction the new Ni-Mon CSMs performed as well as the industry standard Ni-AO with close to full conversion, while Ni-Inc and Ni-CS showed lower but still good activities as high as 53%. Out of the control experiments with untreated Inconel and Monel CSMs, Ni-Mon-UT performed surprisingly well, with conversions as high as 30%; Ni-Inc-UT achieved a maximum of ~8%.

Fig. 8 shows the product distribution for the hydrogenation of the three substrates cinnamaldehyde (CAL), linalool (LOL) and 2,5 dichloro nitrobenzene (DCNB). For CAL, Ni-CS showed the highest activity followed by Ni-AO and the least active CSM Ni-Mon. None of the three catalysts showed high selectivity towards reduction of the alkene over the aldehyde; while Ni-CS reduced a significant amount of the starting material to the fully hydrogenated hydro cinnamyl alcohol (HCOL), the other two produced also smaller amounts of HCOL and some unidentified side products. For the nitro-reduction of DCNB to 2,5-dichloro aniline (DCA), a significant difference in selectivity was observed. While Pd-AO fully reduced the nitro group it also dehalogenated the corresponding aniline to more than 50%, producing monochloro aniline and aniline in the process. For Pt-AO the dehalogenation rate was ~5%. Only the Ni-Mon CSMs were 100% selective towards nitro reduction and did not produce any dehalogenated side products. For the reduction of LOL, which has two C–C double bonds, one internal and one terminal, we could also observe a significant difference in selectivity. The terminal double bond was more reactive in all cases, however only Ni-Mon achieved a ~100% selectivity towards reduction of only the terminal alkene to form 1,2-dihydrolinalool (DHL). Pt-AO produced 6% tetrahydro linalool (THL); Ni-AO produced 38% THL and Pd-AO fully reduced the entire starting material to THL.

To investigate the limits of selectivity for the Monel catalyst, the catalytic hydrogenation of β-myrcene was tested next (see Scheme 1). At a liquid flow rate of 2 mL min^{-1}, 24 bar, 120 °C and an H/S ratio of 5, the Ni-Mon CSMs achieved full conversion, yielding 7% citronellene, 27% 1,2-dihydromyrcene and 65% 2,6-dimethyloct-2-ene, with trace amounts of unidentified side-products. Changing the H/S ratio for this reaction to 1.5 or 15 altered the product composition only insignificantly. The higher amounts of the 1,2-hydrogenated product over the methylene-hydrogenated product citronellene, confirms the selectivity of Ni-Mon for hydrogenation of 1° over 2°-terminal double bonds. However, the high conversion into the tetra-hydrogenated derivative is somewhat surprising, in comparison to the results from the linalool hydrogenation. This can be attributed to the conjugation between these two double bonds, which

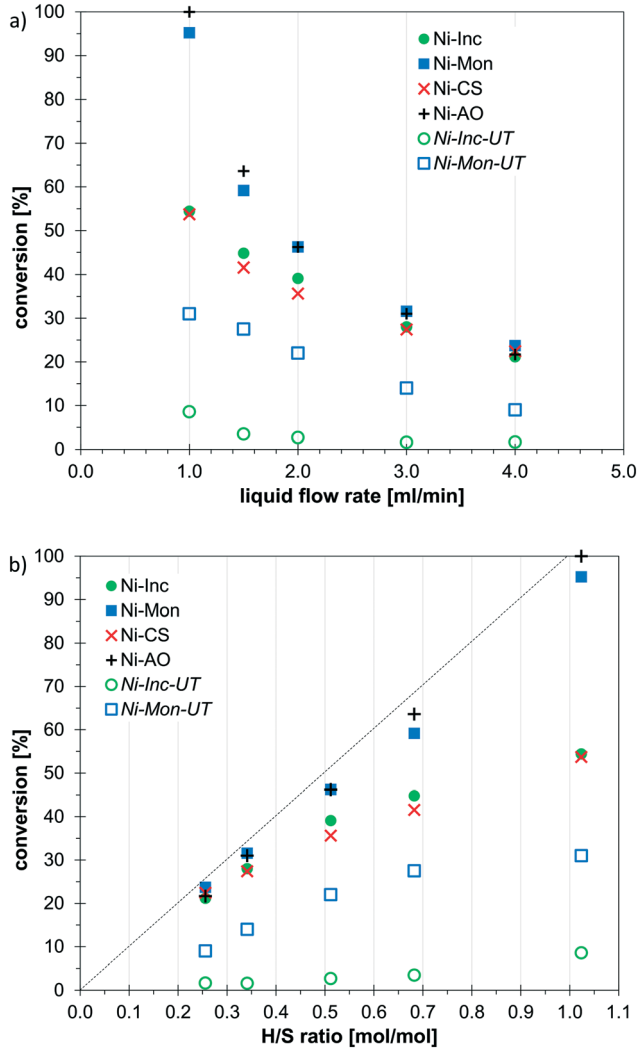

Fig. 7 Conversion plots for hydrogenation of vinyl acetate using different Ni CSMs; a) conversion *vs.* liquid flow rate, b) conversion *vs.* H/S ratio (the dotted line represents the theoretical maximum); the Inconel and Monel CSMs, were tested before (Ni-Inc-UT & Ni-Mon-UT) and after (Ni-Inc & Ni-Mon) the chemical etching/leaching treatment.

increases the likelihood that both undergo hydrogenation. On the other hand, the complete absence of the fully hydrogenated 2,6-dimethyloctane reinforces the steric selectivity of this catalyst. The same reaction at identical conditions over Pd-AO generated only 2,6-dimethyloctane.

In order to investigate the long-term performance of our Ni-Mon catalysts, we conducted an experiment, running the CSM reactor for several hours at a time, for the reduction of myrcene. This experiment was conducted over two days and had an accumulative runtime of 5 h. The reactor performance was evaluated at the beginning and at the end of the experiment using NMR. While at the start the Ni-Mon CSMs achieved a nearly full conversion of myrcene, yielding 65% 2,6-dimethyloct-2-ene; at the end of the runtime the conversion had only very slightly dropped to 98%, yielding 64% 2,6-dimethyloct-2-ene. This experiment shows early data, that these CSMs can achieve stable activity over several hours; for more industrially relevant runtimes, we envisage to conduct time-on-stream experiments for the Ni-Mon CSMs over several days as part of future work.

Our experiments have demonstrated a surprising selectivity profile for these new Ni-Mon CSMs. They are highly active for the reduction of 1°-terminal alkenes (see linalool and myrcene reactions). They have modest to good activity for nitro reductions and for reductions of 2°-terminal double bonds (see myrcene and vinyl acetate reactions), low activity for carbonyl reductions (see cinnamaldehyde reactions), but in comparison poor activity for reductions of internal double bonds (see linalool, myrcene, coumarin and cinnamaldehyde reactions).

To investigate the leaching characteristics of the Ni-Inc and Ni-Mon CSMs, we have conducted a series of long-term reduction experiments whereby a set of 4 CSMs for each type was subjected to an 8 h experiment reducing VAc in ethanol. The entire product solution from each experiment was collected and concentrated, and then a sample was analysed by ICP-OES for its metal content. Table 5 shows these results which represent the metal leaching profile of the CSM reactor during hydrogenation conditions. For both, Ni-Inc and Ni-Mon, noticeable amounts of Ni are detected at levels around 1 ppm. With the exception of Fe, all other metals were detected in much lower quantities of 200 ppb or lower. Interestingly, the Ni-Inc profile showed only 171 ppb of Cr (the second most abundant metal in Inconel 738) and the Ni-Mon profile showed only 26 ppb of Cu (the second most abundant metal in Monel 400). Also, Mn, Ti, Co and Mo were detected in the Ni-Inc profile, all of which are components of Inconel 738; and the same can be said about Mn and Si for Monel 400 and the Ni-Mon samples. However, the by far biggest share of the metal content found in both leaching profiles was Fe, ranging between 3 and 4.6 ppm. This clearly indicates that the majority of the leaching comes from the reactor walls and not from the CSMs themselves, leading to the conclusion that the catalytically active layer is tightly bound to the surface of the mixer. It should further be noted that 316 stainless steel, from which the reactor body, all tubing leading to and from it and most of the process instrumentation are made of, also contains larger amounts of Ni (~12%) and Cr (~17%) and smaller amounts of Mo, Mn and Si. Therefore, the detected contaminants of these metals can also result from the reactor walls. The observation is in strong agreement with all of our previous leaching tests with CSMs containing either electroplated, cold-sprayed or wash coated catalyst layers,[12,27–29,31,32] where Fe was always the major contaminant. Aside from soluble metal impurities, measured by ICP-OES, CSMs can sometimes also produce insoluble metal particles that flake off the catalyst surface during use. For both the Ni-Inc and Ni-Mon CSMs we did not observe any noticeable amounts of insoluble particulate matter, adding to the observation that the active catalytic layer is tightly bound to the mixer scaffold.

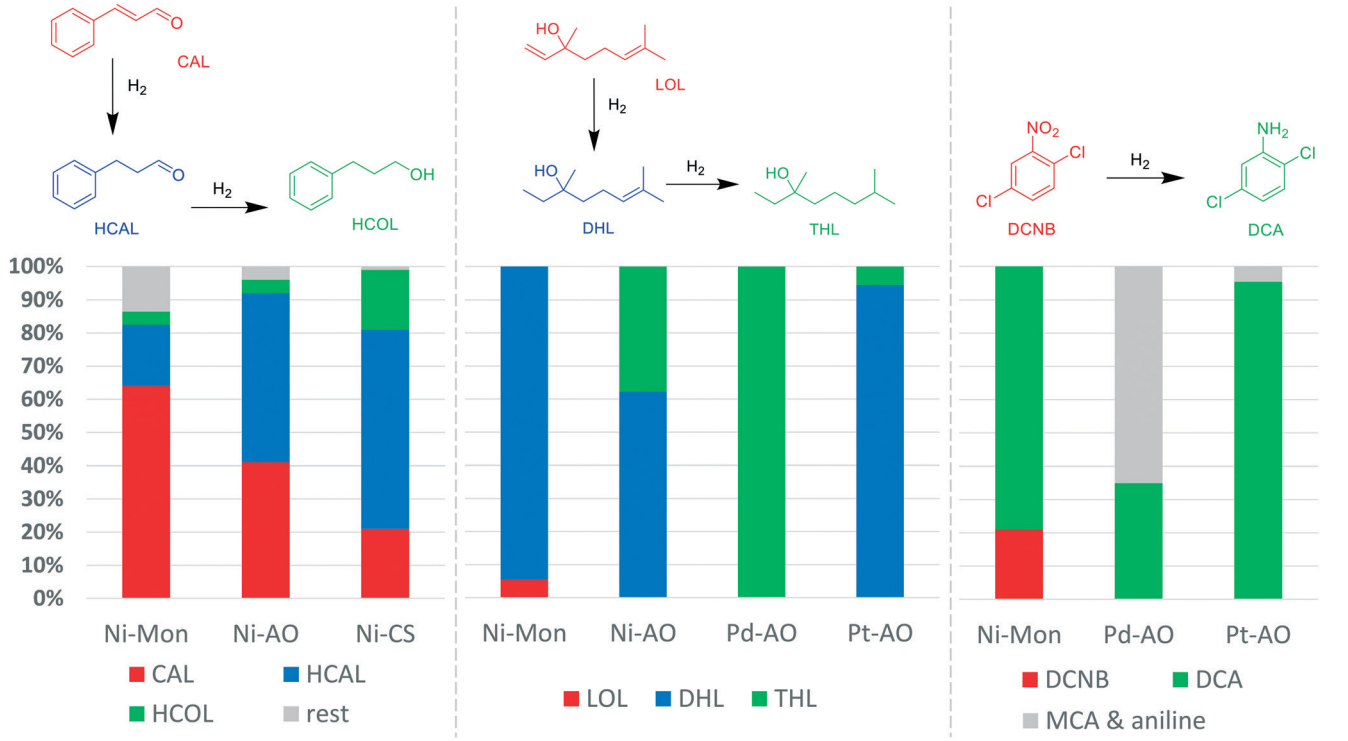

Fig. 8 Hydrogenation pathway of cinnamaldehyde (CAL), yielding, hydrocinnamaldehyde (HCAL) and hydrocinnamyl alcohol (HCOL); cinnamyl alcohol was not observed; hydrogenation pathway of linalool (LOL), yielding 1,2-dihydrolinalool (DHL) and tetrahydrolinalool (THL); 6,7-dihydrolinalool was not observed; hydrogenation pathway of 2,5-dichloro nitrobenzene (DCNB), yielding 2,5 dichloro aniline (DCA) as desired product and monochloro aniline (MCA) and aniline as undesired side-products; product distribution for different CSMs; the experiments were conducted using a liquid flow rate of 2 mL min^{-1} and an H/S ratio of 5 for CAL and LOL and 50 for DCNB; the structure of two observed side products from the cinnamaldehyde reduction could not be fully identified by NMR or GC-MS and are marked here as 'rest'.

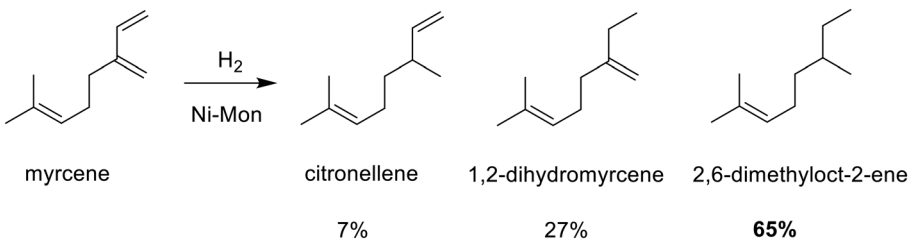

Scheme 1 Hydrogenation of myrcene over Ni-Mon CSMs, yielding citronellene, 1,2-dihydromyrcene and 2,6-dimethyloct-2-ene.

Table 5 Metal leaching profiles of Ni-Inc and Ni-Mon CSMs during hydrogenation conditions; all levels are provided in ppm and were collected from a set of 4 CSMs for the hydrogenation of VAc in ethanol; '*ud*' stands for 'undetected' and denotes that this level was below the detection limit

CSM	Ni	Cu	Cr	Mn	Fe	Al	Ti	Co	Mo	Si
Ni-Inc	1.084	0.006	0.171	0.038	3.042	ud	0.200	0.017	0.076	ud
Ni-Mon	0.880	0.026	0.057	0.109	4.578	0.109	0.010	ud	0.012	0.063

Conclusions

3D printed mixer scaffolds are traditionally combined with coating methods to imbue them with catalytic activity. Herein, we demonstrated the use of chemical etchants and leachants to activate catalytic static mixers printed from Inconel 738 and Monel 400, which are nickel base alloys commonly used in chemical apparatus. It should thus be noted that our work has also shown that chemical reactors built from these materials may suffer from side-reactions due to the presence of these catalytically active surfaces, even without use of an etching or leaching process. Employing the described chemical treatments however, led to a very significant increase in the surface area and the catalytic activity of these CSMs for nickel-catalysed hydrogenation reactions by almost an order of magnitude. In particular,

leaching of the Monel surfaces using a combination of (per-) sulfate solutions led to a significant enrichment of superficial nickel, as characterised by XPS and EDX, which further boosted its catalytic performance to levels comparable with alumina-supported nanoparticulate nickel for certain reductions. The treated Monel surface also displayed high selectivity for the reduction of unsubstituted double bonds: it was never observed to hydrogenate a tri-substituted double bond and showed poor activity for secondary internal bonds, except for myrcene (which is attributed to the internal conjugation of the molecule). The high selectivity of the catalyst even extended to nitro reductions, as the Ni-Mon CSMs were the only catalysts tested that did not dechlorinate 2,5-dichloronitrobenzene in its hydrogenation into 2,5-dichloroanailine.

Contrary to most conventional powder-form or pelletised nickel catalysts, our CSMs consist of a 3D printed scaffold, providing structural integrity, and an activated, porous top layer, both made from the same corrosion resistant nickel base alloy. The manufacturing method is in stark contrast to most other nickel catalysts which often are made from expensive precursors materials and require the use of complex porous support materials, binders, ligands or other additives. Our approach has the potential to be a cost-effective alternative to more complex and expensive nickel or other transition metal catalysts, as the material used to construct these CSMs are standard engineering alloys, rated for use with high corrosive media such as strong acids and bases. Compared to powder form catalysts, employed as slurry systems or packed beds, the CSM technology provides the advantages of low pressure drop and low clogging risk, which is especially important for industrial continuous flow operations.

Our study serves to demonstrate the flexibility of catalytic static mixers and presents proof-of-concept of this subtractive method to from structured catalysts, a relatively unexplored facet of heterogeneous catalysis that likely deserves more attention in the future.

Conflicts of interest

There are no conflicts to declare.

Acknowledgements

The authors thank Borhan Bin Mohamad Sultan for SEM imaging, Winston Liew for ICP-OES measurements, Chris Easton for XPS measurements, Derrick Ng and Tom Grahl for preparing the wash-coated alumina CSMs, Andrew Urban for cold-spraying of the Ni-CS catalyst, Oliver Hutt and Mike Horne for many helpful discussions. The authors also acknowledge financial support from the Science and Industry Endowment Fund (SIEF).

Notes and references

1 J. N. Stuecker, J. E. Miller, R. E. Ferrizz, J. E. Mudd and J. Cesarano, Advanced Support Structures for Enhanced Catalytic Activity, *Ind. Eng. Chem. Res.*, 2004, **43**(1), 51–55, DOI: 10.1021/ie030291v.

2 C. R. Tubío, J. Azuaje, L. Escalante, A. Coelho, F. Guitián, E. Sotelo and A. Gil, 3D Printing of a Heterogeneous Copper-Based Catalyst, *J. Catal.*, 2016, **334**, 110–115, DOI: 10.1016/j.jcat.2015.11.019.

3 D. Albani, G. Vilé, M. A. B. Toro, R. Kaufmann, S. Mitchell and J. Pérez-Ramírez, Structuring Hybrid Palladium Nanoparticles in Metallic Monolithic Reactors for Continuous-Flow Three-Phase Alkyne Hydrogenation, *React. Chem. Eng.*, 2016, **1**(4), 454–462, DOI: 10.1039/C6RE00114A.

4 C. Hurt, M. Brandt, S. S. Priya, T. Bhatelia, J. Patel, P. Selvakannan and S. Bhargava, Combining Additive Manufacturing and Catalysis: A Review, *Catal. Sci. Technol.*, 2017, **7**(16), 3421–3439, DOI: 10.1039/C7CY00615B.

5 S. Rossi, A. Puglisi and M. Benaglia, Additive Manufacturing Technologies: 3D Printing in Organic Synthesis, *ChemCatChem*, 2018, **10**(7), 1512–1525, DOI: 10.1002/cctc.201701619.

6 C. Parra-Cabrera, C. Achille, S. Kuhn and R. Ameloot, 3D Printing in Chemical Engineering and Catalytic Technology: Structured Catalysts, Mixers and Reactors, *Chem. Soc. Rev.*, 2018, **47**(1), 209–230, DOI: 10.1039/C7CS00631D.

7 A. S. Díaz-Marta, C. R. Tubío, C. Carbajales, C. Fernández, L. Escalante, E. Sotelo, F. Guitián, V. L. Barrio, A. Gil and A. Coelho, Three-Dimensional Printing in Catalysis: Combining 3D Heterogeneous Copper and Palladium Catalysts for Multicatalytic Multicomponent Reactions, *ACS Catal.*, 2018, **8**(1), 392–404, DOI: 10.1021/acscatal.7b02592.

8 A. Sanchez Díaz-Marta, S. Yáñez, C. R. Tubío, V. L. Barrio, Y. Piñeiro, R. Pedrido, J. Rivas, M. Amorín, F. Guitián and A. Coelho, Multicatalysis Combining 3D-Printed Devices and Magnetic Nanoparticles in One-Pot Reactions: Steps Forward in Compartmentation and Recyclability of Catalysts, *ACS Appl. Mater. Interfaces*, 2019, **11**(28), 25283–25294, DOI: 10.1021/acsami.9b08119.

9 E. Lahtinen, L. Turunen, M. M. Hänninen, K. Kolari, H. M. Tuononen and M. Haukka, Fabrication of Porous Hydrogenation Catalysts by a Selective Laser Sintering 3D Printing Technique, *ACS Omega*, 2019, **4**(7), 12012–12017, DOI: 10.1021/acsomega.9b00711.

10 M. R. Penny and S. T. Hilton, Design and Development of 3D Printed Catalytically-Active Stirrers for Chemical Synthesis, *React. Chem. Eng.*, 2020, **5**(5), 853–858, DOI: 10.1039/C9RE00492K.

11 X. Wang, W. Guo, R. Abu-Reziq and S. Magdassi, High-Complexity WO3-Based Catalyst with Multi-Catalytic Species via 3D Printing, *Catalysts*, 2020, **10**(8), 840, DOI: 10.3390/catal10080840.

12 M. Kundra, B. Bin Mohamad Sultan, D. Ng, Y. Wang, D. L. J. Alexander, X. Nguyen, Z. Xie and C. H. Hornung, Continuous Flow Semi-Hydrogenation of Alkynes Using 3D Printed Catalytic Static Mixers, *Chem. Eng. Process.*, 2020, **154**, 108018, DOI: 10.1016/j.cep.2020.108018.

13 S. Lawson, A. Farsad, B. Adebayo, K. Newport, K. Schueddig, E. Lowrey, F. Polo-Garzon, F. Rezaei and A. A.

Rownaghi, A Novel Method of 3D Printing High-Loaded Oxide/H-ZSM-5 Catalyst Monoliths for Carbon Dioxide Reduction in Tandem with Propane Dehydrogenation, *Adv. Sustainable Syst.*, 2021, **5**(3), 2000257, DOI: 10.1002/adsu.202000257.

14 R. M. Ferrizz, J. N. Stuecker, J. Cesarano and J. E. Miller, Monolithic Supports with Unique Geometries and Enhanced Mass Transfer, *Ind. Eng. Chem. Res.*, 2005, **44**(2), 302–308, DOI: 10.1021/ie049468r.

15 M. D. Symes, P. J. Kitson, J. Yan, C. J. Richmond, G. J. T. Cooper, R. W. Bowman, T. Vilbrandt and L. Cronin, Integrated 3D-Printed Reactionware for Chemical Synthesis and Analysis, *Nat. Chem.*, 2012, **4**(5), 349–354, DOI: 10.1038/nchem.1313.

16 Y. Elias, P. Rudolf von Rohr, W. Bonrath, J. Medlock and A. Buss, A Porous Structured Reactor for Hydrogenation Reactions, *Chem. Eng. Process.: Process Intesif.*, 2015, **95**, 175–185, DOI: 10.1016/j.cep.2015.05.012.

17 S. Danaci, L. Protasova, J. Lefevere, L. Bedel, R. Guilet and P. Marty, Efficient CO2 Methanation over Ni/Al2O3 Coated Structured Catalysts, *Catal. Today*, 2016, **273**, 234–243, DOI: 10.1016/j.cattod.2016.04.019.

18 M. Konarova, W. Aslam, L. Ge, Q. Ma, F. Tang, V. Rudolph and J. N. Beltramini, Enabling Process Intensification by 3 D Printing of Catalytic Structures, *ChemCatChem*, 2017, **9**(21), 4132–4138, DOI: 10.1002/cctc.201700829.

19 J. Azuaje, C. R. Tubío, L. Escalante, M. Gómez, F. Guitián, A. Coelho, O. Caamaño, A. Gil and E. Sotelo, An Efficient and Recyclable 3D Printed α-Al2O3 Catalyst for the Multicomponent Assembly of Bioactive Heterocycles, *Appl. Catal., A*, 2017, **530**, 203–210, DOI: 10.1016/j.apcata.2016.11.031.

20 X. Li, F. Rezaei and A. A. Rownaghi, Methanol-to-Olefin Conversion on 3D-Printed ZSM-5 Monolith Catalysts: Effects of Metal Doping, Mesoporosity and Acid Strength, *Microporous Mesoporous Mater.*, 2019, **276**, 1–12, DOI: 10.1016/j.micromeso.2018.09.016.

21 F. Magzoub, X. Li, J. Al-Darwish, F. Rezaei and A. A. Rownaghi, 3D-Printed ZSM-5 Monoliths with Metal Dopants for Methanol Conversion in the Presence and Absence of Carbon Dioxide, *Appl. Catal., B*, 2019, **245**, 486–495, DOI: 10.1016/j.apcatb.2019.01.008.

22 A. Sanchez Díaz-Marta, S. Yáñez, C. R. Tubío, V. L. Barrio, Y. Piñeiro, R. Pedrido, J. Rivas, M. Amorín, F. Guitián and A. Coelho, Multicatalysis Combining 3D-Printed Devices and Magnetic Nanoparticles in One-Pot Reactions: Steps Forward in Compartmentation and Recyclability of Catalysts, *ACS Appl. Mater. Interfaces*, 2019, **11**(28), 25283–25294, DOI: 10.1021/acsami.9b08119.

23 O. A. Alimi, C. A. Akinnawo and R. Meijboom, Monolith Catalyst Design via 3D Printing: A Reusable Support for Modern Palladium-Catalyzed Cross-Coupling Reactions, *New J. Chem.*, 2020, **44**(43), 18867–18878, DOI: 10.1039/D0NJ03651J.

24 E. Bulatov, E. Lahtinen, L. Kivijärvi, E. Hey-Hawkins and M. Haukka, 3D Printed Palladium Catalyst for Suzuki-Miyaura Cross-Coupling Reactions, *ChemCatChem*, 2020, **12**(19), 4831–4838, DOI: 10.1002/cctc.202000806.

25 C. Y. Chaparro-Garnica, P. Jordá-Faus, E. Bailón-García, R. Ocampo-Pérez, C. G. Aguilar-Madera, A. Davó-Quiñonero, D. Lozano-Castelló and A. Bueno-López, Customizable Heterogeneous Catalysts: Nonchanneled Advanced Monolithic Supports Manufactured by 3D-Printing for Improved Active Phase Coating Performance, *ACS Appl. Mater. Interfaces*, 2020, **12**(49), 54573–54584, DOI: 10.1021/acsami.0c14703.

26 T. Li, J. Gonzalez-Gutierrez, I. Raguž, C. Holzer, M. Li, P. Cheng, M. Kitzmantel, L. Shi and L. Huang, Material Extrusion Additively Manufactured Alumina Monolithic Structures to Improve the Efficiency of Plasma-Catalytic Oxidation of Toluene, *Addit. Manuf.*, 2021, **37**, 101700, DOI: 10.1016/j.addma.2020.101700.

27 M. Kundra, T. Grall, D. Ng, Z. Xie and C. H. Hornung, Continuous Flow Hydrogenation of Flavorings and Fragrances Using 3D-Printed Catalytic Static Mixers, *Ind. Eng. Chem. Res.*, 2021, **60**(5), 1989–2002, DOI: 10.1021/acs.iecr.0c05671.

28 C. H. Hornung, X. Nguyen, A. Carafa, J. Gardiner, A. Urban, D. Fraser, M. D. Horne, D. R. Gunasegaram and J. Tsanaktsidis, Use of Catalytic Static Mixers for Continuous Flow Gas–Liquid and Transfer Hydrogenations in Organic Synthesis, *Org. Process Res. Dev.*, 2017, **21**(9), 1311–1319, DOI: 10.1021/acs.oprd.7b00180.

29 J. Gardiner, X. Nguyen, C. Genet, M. D. Horne, C. H. Hornung and J. Tsanaktsidis, Catalytic Static Mixers for the Continuous Flow Hydrogenation of a Key Intermediate of Linezolid (Zyvox), *Org. Process Res. Dev.*, 2018, **22**(10), 1448–1452, DOI: 10.1021/acs.oprd.8b00153.

30 R. Lebl, Y. Zhu, D. Ng, C. H. Hornung, D. Cantillo and C. O. Kappe, Scalable Continuous Flow Hydrogenations Using Pd/Al2O3-Coated Rectangular Cross-Section 3D-Printed Static Mixers, *Catal. Today*, 2022, **383**, 55–63, DOI: 10.1016/j.cattod.2020.07.046.

31 A. Avril, C. H. Hornung, A. Urban, D. Fraser, M. Horne, J.-P. Veder, J. Tsanaktsidis, T. Rodopoulos, C. Henry and D. R. Gunasegaram, Continuous Flow Hydrogenations Using Novel Catalytic Static Mixers inside a Tubular Reactor, *React. Chem. Eng.*, 2017, **2**(2), 180–188, DOI: 10.1039/C6RE00188B.

32 C. Genet, X. Nguyen, B. Bayatsarmadi, M. D. Horne, J. Gardiner and C. H. Hornung, Reductive Aminations Using a 3D Printed Supported Metal(0) Catalyst System, *J. Flow Chem.*, 2018, **8**(2), 81–88, DOI: 10.1007/s41981-018-0013-6.

33 L. E. Murr, A Metallographic Review of 3D Printing/Additive Manufacturing of Metal and Alloy Products and Components, *Metallogr., Microstruct., Anal.*, 2018, **7**(2), 103–132, DOI: 10.1007/s13632-018-0433-6.

34 M. Xia, D. Gu, G. Yu, D. Dai, H. Chen and Q. Shi, Selective Laser Melting 3D Printing of Ni-Based Superalloy: Understanding Thermodynamic Mechanisms, *Sci. Bull.*, 2016, **61**(13), 1013–1022, DOI: 10.1007/s11434-016-1098-7.

35 A. Ramakrishnan and G. P. Dinda, Direct Laser Metal Deposition of Inconel 738, *Mater. Sci. Eng., A*, 2019, **740–741**, 1–13, DOI: 10.1016/j.msea.2018.10.020.
36 Metallographic Etchants https://www.metallographic.com/Metallographic-Etchants/Metallography-Etchants.htm (accessed 2021 -06 -06).
37 F. Bari, N. Begum, S. B. Jamaludin and K. Hussin, Selective Leaching For The Recovery Of Copper From PCB.
38 G. C. Bond, *Metal-Catalysed Reactions of Hydrocarbons; Fundamental and applied catalysis*, Kluwer Academic/Plenum Publishers, New York, 2005.